ChemComm

Accepted Manuscript

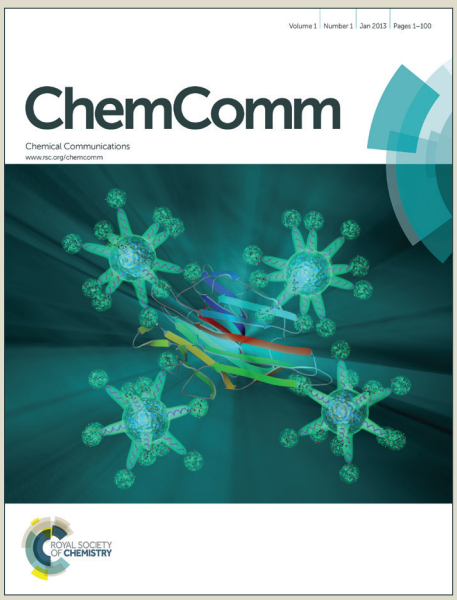

ROYAL SOCIETY OF CHEMISTRY

www.rsc.org/chemcomm

ChemComm

RSCPublishing

COMMUNICATION

Core-Shell Nanohollow-γ-Fe_2O_3@Graphene Hybrid Prepared through the Kirkendall Process as High Performance Anode Materials for Lithium Ion Battery

Cite this: DOI: 10.1039/xoxxoooooox

Received ooth January 2012,
Accepted ooth January 2012

DOI: 10.1039/xoxxoooooox

www.rsc.org/

Jiangtao Hu‡, Jiaxin Zheng‡, Leilei Tian, Yandong Duan, Lingpiao Lin, Suihan Cui, Hao Peng, Tongchao Liu, Hua Guo, Xinwei Wang, and Feng Pan*

We synthesized a core-shell structure with graphene as the shell and nano-hollow γ-Fe_2O_3 as the core through a Kirkendall process at room temperature. When the hybrids are served as anode materials for lithium-ion batteries, they exhibit remarkable electrochemical performance: a high reversible capacity of 1095, 833, and 551mAhg^{-1} at the current rates of 0.1 C, 1 C, and 2 C, respectively. When evaluated at 10 C, the capacity still can reach 504mAhg^{-1}.

Lithium ion batteries (LIBs) have captured extensive applications in hybrid electric vehicles, electric vehicles, and portable electronic devices, etc.[1] Due to their high theoretical and experimental specific capacity, metal oxides, such as Co_3O_4,[2] NiO,[3] SnO_2,[4] Bi_2O_3,[5] GeO_2,[6] CuO,[7] Fe_3O_4,[8] and Fe_2O_3,[9] have been widely investigated as candidates for advanced anode materials. Particularly, with substantial merits of high capacity, environment friendliness, widespread availability, and enhanced safety, iron oxides are now one of the most promising anodes.[10] However, iron oxides generally bear capacity fading during cycling for its large volume expansion in charge/discharge processes and low rate capacity caused by its poor electronic conductivity.[11] The large volume changes of these anode particles would break the solid electrolyte interface (SEI) and make it re-grown at the solid-liquid interfaces during the cycling, leading to poor cycling stability with the Li-ion and electrolyte solution depletion.

One strategy which succeeds to improve the SEI stability was to create core-shell or yoke-shell structures, in which the nano-core particles can only expand toward the inside of the shell and the hollows of these core-shell structures are able to balance the volume changes.[12] Thus, to prepare iron oxides with nano-hollow structures to release the stress during volume expansion would be a good way to enhance the cycling performance. There are several well developed approaches (removable templates or template-free) to generate hollow micro/nanostructures. Among of them, the Kirkendall effect,[13] which is caused by the differences for diffusion directions and speeds between different ions in the synthesis process, is demonstrated to be a simple, effective, and template-free method. To improve the electronic conduction of these metal oxides, carbon coating on the particle surfaces is a most widely used method.[14] The two dimensional graphene is a well-known carbon allotrope, which possesses high electron mobility and good structure flexibility.[15] Mixing iron oxides with graphene would not only form an electrical conductive network in the anode composite to improve the electrical conductivity greatly but also protect the structure stability in the charge/discharge process. Moreover, the graphene could contribute to the total energy storage by its capacitance. However, the final improvement of electrochemical performance introduced by the mixed graphene depends on the mixing or coating way.

Prussian blue (PB) is one of an important class of crystalline inorganic-organic hybrids coordinated to rigid organic molecules, which can be used as a novel precursor to prepare various porous micro/nanostructures from zero- to three-dimension.[16] In this communication, we report a novel method to prepare the core-shell structure with graphene as the shell and nano-hollow γ-Fe_2O_3 as the core (core-shell nano-hollow-γ-Fe_2O_3@graphene) through the nano-scale Kirkendall effect at room temperature. PB is employed as a precursor, and the shell graphene layers are formed on the surface of nano iron particles, which is reduced by glucose with Ar during the heating process. When served as anode materials for lithium-ion secondary battery, the hybrid anode shows remarkable electrochemical performance: a high reversible capacity of 1095, 833, and 551mAhg^{-1} at the current rates of 0.1 C, 1 C, and 2 C after 100 cycles, respectively. When evaluated at 10 C, the capacity still can reach 504 mAhg^{-1}.

The core-shell nanohollow γ-Fe_2O_3@graphene was prepared as the following steps (Scheme 1): The prepared PB precursors were calcined at 650 ^oC in argon atmosphere, and Fe nano-metals were produced by reduction of glucose decomposition (Step I). After the furnace cooling naturally to room temperature and then exposing in air, graphene shells were formed and Fe nano-particles were then oxidized by O_2 by a spontaneous combustion to be transferred into nano-hollow γ-Fe_2O_3 (Step II and III). As a reference, α-Fe_2O_3 was also synthesized by calcining the mixture of PB/glucose in air atmosphere at 650 ^oC (Fig. S1).

The crystalline structures of the prepared samples were first characterized by X-ray diffraction using Cu Kα radiation (λ =0.15418 nm) (Fig. 1a). The diffraction peaks at 30.24, 35.63, 43.28, 53.73, 57.27, 62.925, and 62.499° corresponding to crystalline planes of (022), (311), (400), (422), (511), and (440) can be assigned

to γ-Fe_2O_3 or Fe_3O_4 (JCPDS No. 39-1346, lattice constant a=b=c=0.83515 nm).

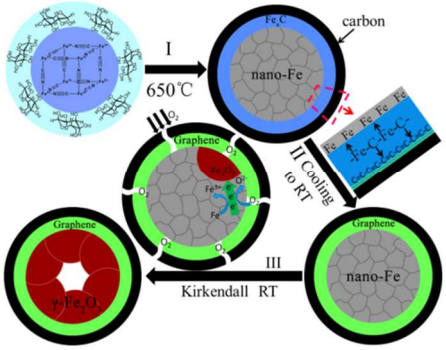

Scheme 1. The schematic illustration of the preparation of the nano-hollow γ-Fe_2O_3@graphene hybrid. (RT: Room Temperature).

The XPS peaks of Fe $2p_{3/2}$ and $Fe2p_{1/2}$ for the material are shown in Fig. S2a. The peak position of Fe $2p_{3/2}$ is 710.6 eV, which has been reported previously.[17] There is a satellite peak of Fe $2p_{3/2}$ located at 8 eV higher than the main Fe $2p_{3/2}$ peak[18], indicating that the material contains Fe^{3+} but no Fe^{2+}. Therefore, the prepared samples are proved to be γ-Fe_2O_3. The γ-Fe_2O_3 is a nested structure containing FeO_4 tetrahedrons and FeO_6 hexahedrons, and the (400) peak relates to the face crossing the FeO_4 tetrahedrons (Fig. 1b).

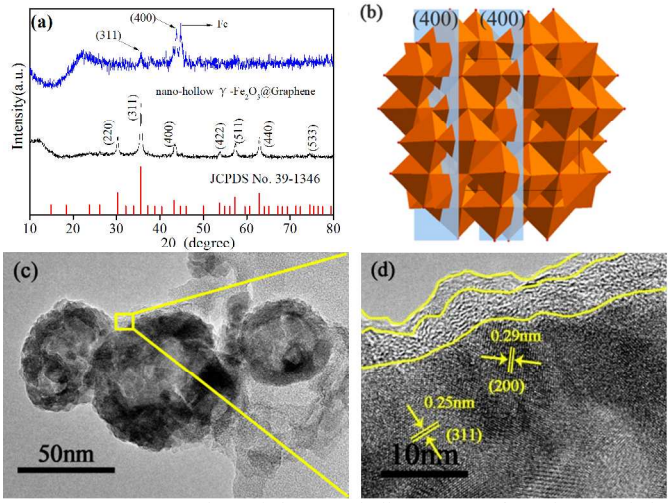

Figure 1. (a) XRD data of the nano-hollow γ-Fe_2O_3@graphene and the intermediate state; (b) the crystal structure of γ-Fe_2O_3; (c) and (d) TEM images of the nano-hollow γ-Fe_2O_3@graphene.

The morphology of the γ-Fe_2O_3 particles characterized by TEM, with sizes of about 40-60nm, are shown in Fig. 1c and 1d. Noticeably, it shows a core-shell and nano-hollow structure. The core contains many γ-Fe_2O_3 cells (Fig. 1d), which is determined to be about 19 nm by using Scherrer equation to the strongest (311) diffraction peak. The Raman spectrum of the nano-hollow γ-Fe_2O_3 hybrid is shown in Fig. 2a. There are two characteristic peaks at 1360 and 1600 cm^{-1}, respectively, corresponding to the D band and G band of carbon (I_D:I_G = 1.0056). The D-band illustrates the defects and disordered portions of carbon, while G-band stands for the order graphitic crystallites of carbon. The high resolution C1s XPS spectrum of the composite (Fig. 2b) can be fitted into five components, corresponding to carbon atoms in five different chemical environments: carbon sp^2 (284.4eV), carbon sp^3 (285.2eV), the carbon in C-O (286.2eV), the carbonyl carbon (C=O) at 287.9eV, the caboxylate carbon (O-C=O) at 289.0 eV.[19] The percentage of carbon sp^2 is 40.6%, indicating a high graphitization degree. Therefore, large amounts of graphene-like carbon fragments are formed as the shell on the core nano-hollow γ-Fe_2O_3 particles. When we place the nano-hollow γ-Fe_2O_3@graphene in concentrated hydrochloric acid, the nano-hollow γ-Fe_2O_3 is dissolved and the nano carbon shell is left (Fig. S2b), indicating the material with a stable shell structure. From the TEM images of such shell structures (Fig. 2c and 2d), we can see clearly that the shell consists of thin layers with several nanometers thick. A large weight loss of γ-Fe_2O_3@graphene about 17.02 % between 300 and 450℃ could be seen from the TGA curve (Fig. S3b), which can be ascribed to the combustion of graphene with amorphous carbon coated on nano-hollow γ-Fe_2O_3 particles.

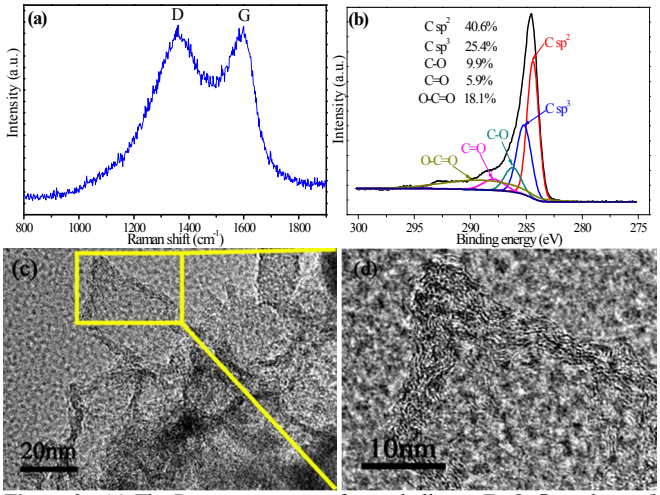

Figure 2. (a) The Raman spectrum of nano-hollow γ-Fe_2O_3@graphene; (b) C1s spectra of nano-hollow γ-Fe_2O_3@graphene. (c and d) TEM images of the shell of the graphene left from nano-hollow γ-Fe_2O_3 @graphene dissolved in HCl.

Interestingly, the (400) faces are well aligned around and perpendicular to the shell layer of γ-Fe_2O_3 particles (keeping near 90° degree with the layer), as shown in Fig. 1d, which would facilitate the Li-ion intercalation/de-intercalation along the (400) planes. To further survey the pore size distribution (PSD) and specific surface area for nano-hollow γ-Fe_2O_3, Nitrogen isothermal adsorption measurements were performed (Fig. S3c and S3d). The isothermal curves are regarded as an International Union of Pure and Applied Chemistry (IUPAC) IV type curve, indicating numerous inhomogeneous nanoscale nanoporous and mesoporous in the samples with large specific surface area. EDS element mapping is shown in Fig. S4a, and the three elements distribute uniformly in this hybrids. The BET specific surface area of the nano-hollow γ-Fe_2O_3@graphene is 203.24 m^2g^{-1}. It is apparent that the specific surface areas of the mesoporous Fe_2O_3 are much larger than the solid core Fe_2O_3. Such higher surface areas can be attributed to the novel core-shell and nano-hollow structure.

Previous literatures also reported nano-hollow Fe_2O_3 can be obtained by direct decomposition of prussian blue particles. For example, Hu et al. first synthesized hollow PB precursors and then sintered them at 250℃ in air to get γ-Fe_2O_3 with hollow structures;[20] Zhang et al. first used the prepared PB to react with NaOH solution with different concentrations at room temperature to get $Fe(OH)_3$ microboxes with controllable multishelled structure[21]. Then they sintered the $Fe(OH)_3$ microboxes at 300℃ in air to get γ-Fe_2O_3 with hollow structures. Different from the above two methods, we synthesized the hollow γ-Fe_2O_3 through a simple Kirkendall effect at room temperature. We just sinter the prepared solid PB particles at 650 ℃ in Argon and then cool the products naturally to room temperature in air. The SEM images of the PB precursor and nano-hollow γ-Fe_2O_3 particles are shown in Fig. S4, we can see that the particle size of PB became smaller (half of the original) after

sintered at 650℃ in Argon. In order to clarify the synthesis process of nano-hollow γ-Fe_2O_3, we took the crucible out of quartz tube, and then poured a right amount of alcohol into the crucible to protect O_2 without further oxidation and detected the structure using XRD immediately. Interestingly, the iron peak was observed clearly (Fig. 1a), which explains the spontaneous combustion phenomenon in accordance with the Kirkendall effect with the process (Scheme 1III). The Fe atoms first diffuse toward outside, forming an iron layer. At the same time, when the sintered products are contacted with the air, oxygen ions would diffuse from the surface toward the inside and oxidize the iron atoms to form γ-Fe_2O_3 layer on the iron layer. Due to the different diffusion coefficient for Fe atoms and oxygen ions, the nano-hollow structures were produced. The mechanism for the graphene shell formation can be explained as following: when Prussian blue is gradually transformed into nanometer iron during the heating process (Scheme 1I and 1II), glucose was decomposed into carbon at the same time, and carbon atoms will gradually seep into the nano iron surface and form carburizing solid solution (Fe_xC, $0<x<3$) under the high temperature. During the cooling process, carbon atoms would separate out from the carburizing solid solution and form graphene layers on the surface of iron nanoparticles.[22] This graphene shell structure will be kept when the iron nanoparticles are further oxidized to nano-hollow γ-Fe_2O_3.

We next study the electrochemical properties of such core-shell and nano-hollow γ-Fe_2O_3@graphene composites. The CV curves and the charge-discharge voltage profiles of nano-hollow γ-Fe_2O_3@graphene electrode were shown in Fig. S5a and S5b. Three obvious plateaus can be observed in the first discharge curve, which agrees well with the three peaks in CV results for the first cycle. The following sloping region can be described as the formation of polymeric SEI layers. The first cycle discharge and charge capacities of nano-hollow γ-Fe_2O_3@graphene electrode at 0.1C (1 C = 1000 mAg^{-1}) are 1462.32 and 990.45 $mAhg^{-1}$, respectively, corresponding to a coulombic efficiency of 67.73 %, which can also be explained by the irreversible formation of the SEI layers on the surface of nano-hollow γ-Fe_2O_3@graphene particles.

Table 1. The comparison of iron-based materials for lithium-ion batteries.

	Material (G:graphene)	Specific capacity ($mAhg^{-1}$)	Rate-capacity ($mAhg^{-1}$)
Ref.[24(a)]	Fe_2O_3/C	0.05C/623 for 100cycles	1C/450
Ref.[24(b)]	Fe_2O_3/C	0.2C/790 for 100cycles	4C/390
Ref.[24(c)]	Fe_2O_3/C	0.5C/800 for 100cycles	3C/420
Ref.[24(d)]	Fe_2O_3/G	0.8C/711for 50cycles	1.6C/660
Ref.[24(e)]	Fe_2O_3/G	0.2C/1049for 450cycles	2C/634

Rate capabilities were examined next (Fig. 3a and 3b). Nano-hollow γ-Fe_2O_3@graphene shows rather high rate performance with an average discharge capacity of 1095, 1072, 1022, 974, 902, 704, and 504 mAh g^{-1} at the rate of 0.1, 0.2, 0.5, 1, 2, 5, and 10 C, respectively. These values are much higher than the capacities of γ-Fe_2O_3 reported in other literatures[23] (Fig. 3a) and other Fe_2O_3 anodes (including α-Fe_2O_3) at the same current densities (Tab. 1[24] and Tab. S1). Clear voltage platforms are observed in all the charge and discharge curves (Fig. 3b), corresponding to the process of Li intercalation and de-intercalation. Such excellent rate performance for γ-Fe_2O_3@graphene can be attributed to the structure stability induced by the hollow structure and γ-Fe_2O_3 itself, and the high electrical conductivity induced by the graphene shells. This is also validated by our electrochemical impedance spectroscopy (EIS) measurements (Fig. S6). The cycling performance of nano-hollow γ-Fe_2O_3@graphene and α-Fe_2O_3 within a voltage window of 0.01 to 3 V is illustrated in Fig. S7. The nano-hollow γ-Fe_2O_3@graphene electrode reserved 833 and 551 $mAhg^{-1}$ after 100 cycles at the current rate of 1 and 2C, respectively, demonstrating a good cycle stability.

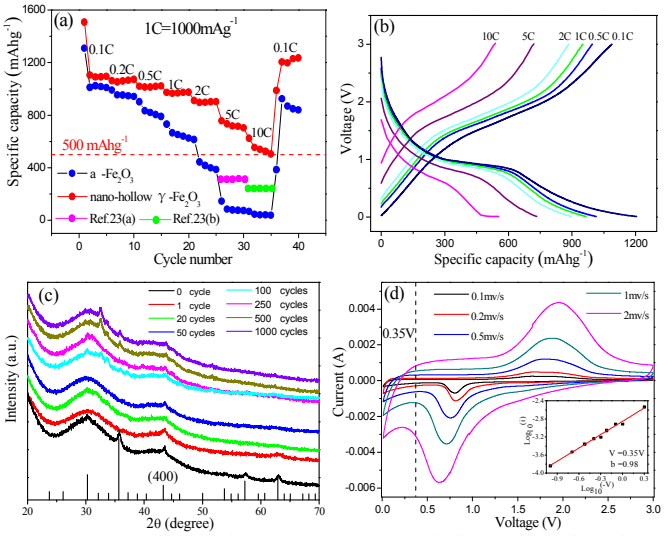

Figure 3. Electrochemical performance for nano-hollow γ-Fe_2O_3@graphene: (a) Rate performances and compared with α-Fe_2O_3, γ-Fe_2O_3@CNTs at 5C, and γ-Fe_2O_3/rGO hybrids at 10C; (b) the charge-discharge curves; (c) XRD datas after different cycles; (d) cyclic voltammograms at different sweep rates. The peaks of CV reflect the redox reactions occurred during the electrochemical process but can't reflect the capacitive properties of the battery, so we randomly selected a voltage point (0.35V) below the peak values and fit the corresponding the logarithmic relationship of sweep rate and current at this point to derive the capacitive properties (inset).

Interestingly, the (400) peak which is related to the planes crossing the FeO_4 tetrahedrons in XRD still exists after 1000 cycles (Fig. 3c), indicating a relatively high structure stability for γ-Fe_2O_3 during the electrochemical cycles. The battery was tested 750 cycles at 10C, and a capacity of 625 $mAhg^{-1}$ was remained when cycled back to 1 C (Fig. S8). The (400) peak in γ-Fe_2O_3 was reported previously [25], but this work is the first time to report that it still exists during charge and discharge process. This structure stability guarantees the cycling stability with fast Li-ion transport. In contrast, the capacity of α-Fe_2O_3 electrode drops heavily during the cycles in our work (400 $mAhg^{-1}$ after 100 cycles at the current rate of 1 C, Fig. S7a) and in Ref. 22(a). The much better cycling stability for the nano-hollow γ-Fe_2O_3@graphene can be attributed to the structure stability for γ-Fe_2O_3 (the (400) peak still exists during charge and discharge process) and the nano-hollow structure with graphene shells, which buffer the volume expansion during electrochemical cycles. While the structure of α-Fe_2O_3 was damaged by the volume expansion during charge and discharge cycles, due to the absence of hollow structures and the relatively low structure stability for α-Fe_2O_3 during the electrochemical cycles.

The cycle capacity of γ-Fe_2O_3@graphene is about 1050$mAhg^{-1}$ at 0.1C (Fig. S9), and γ-Fe_2O_3 can contribute 835.81 $mAhg^{-1}$ (83% in weight). The left part could be ascribed to the capacitance from the carbon (graphene and amorphous carbon，17% in weight in this composite), which is estimated to be 1260 $mAhg^{-1}$. In fact, we can divide the discharge capacity into two parts by 0.8V (Fig. S7b) and plot the capacity for the two parts with the increasing cycle number in Fig. S9. The capacity above 0.8 V denotes the capacity within the discharge platform, and the capacity below 0.8 V denotes the capacity for the tails in the discharge curve. We can see that the capacity above 0.8V is on the way down, the capacity under 0.8V is on the rise with the increasing cycle number. In order to explain this phenomenon, we did a CV test under different rates (Fig. 3d). Assuming that the current obeys a power-law relationship ($i = av^b$), where a and b are adjustable values.[26] If the value of b is equal to 0.5, then we can say the current is controlled by semi-infinite diffusion. If b is equal to 1, it reflects a capacitive process. Here we got the *b*-

value of 0.98 through fitting the logarithmic relationship of sweep rate and current at 0.35V (inset in Fig. 3d), demonstrating that capacitance plays an important role at low voltage (0.8-0.1V) during the discharge process. We attribute this large contribution from capacitance to the graphene shells around the nano-hollow γ-Fe_2O_3@graphene particles and the huge specific surface areas.

Conclusions

In summary, the nano-hollow γ-Fe_2O_3@graphene with a core-shell structure has been synthesized through the Kirkendall process at room temperature. When served as anode materials for LIBs, this hybrid demonstrated a remarkable electrochemical performance: a high reversible capacity of 1095, 833, and 551mAhg^{-1} at the current rates of 0.1 C, 1 C, and 2 C after 100 cycles, respectively. When evaluated at 10 C, the capacity still can reach 504mAhg^{-1}. This remarkable performance can be attributed to the novel nano-hollow and core-shell structure and the structure stability for γ-Fe_2O_3 ((400) peak exists all the time). At the same time, the huge contribution of capacitance is verified, which could be ascribed to the huge specific surface and the tightly coated graphene layers. This synthetic route is simple, low-cost, eco-friendly, and especially, combining Li storage with capacitance in energy storage. It enables the modified γ-Fe2O3 to be a promising anode material for advanced LIBs.

Acknowledgements

This research was supported by National Project for EV Batteries (20121110, OptimumNano, Shenzhen), Guangdong Innovation Team Project (No. 2013N080), NSFC (51302007) and Shenzhen Science and Technology Research Grant (No. ZDSY20130331145131323, CXZZ20120829172325895, JCYJ20120614150338154, and JCYJ20130329181509637).

Notes and references

School of Advanced Materials, Peking University, Peking University Shenzhen Graduate School, Shenzhen 518055, China. Tel: 86-755-26033200; E-mail: panfeng@pkusz.edu.cn.

‡ J. Hu and J. Zheng contributed equally to this work.

Electronic Supplementary Information (ESI) available: [Details of experimental procedures, XRD patterns, XPS analysis, SEM images, TGA curves, N_2 adsorption results, SEM images and electrochemical testing]. See DOI: 10.1039/c000000x/

1 (a) A. Yoshino, *Angew. Chem. Int. Edit.*, 2012, **51**, 5798; (b) P. G. Bruce, B. Scrosati and J. M. Tarascon, *Angew. Chem. Int. Edit.*, 2008, **47**, 2930.
2 B. Li, H. Cao, J. Shao, G. Li, M. Qu and G. Yin, *Inorg. Chem.*, 2011, **50**, 1628.
3 B. Varghese, M. V. Reddy, Y. Zhu, C. S. Lit, T. C. Hoong, G. V. Subba Rao, B. V. R. Chowdari, A. T. S. Wee, C. T. Lim and C. H. Sow, *Chem. Mater.*, 2008, **20**, 3360.
4 C. Kim, M. Noh, M. Choi, J. Cho and B. Park, *Chem. Mater.*, 2005, **17**, 3297.
5 Y. Li, M. A. Trujillo, E. Fu, B. Patterson, L. Fei, Y. Xu, S. Deng, S. Smirnov and H. Luo, *J. Mater. Chem. A*, 2013, **1**, 12123.
6 Y.-M. Lin, K. C. Klavetter, A. Heller and C. B. Mullins, *J. Mater. Chem. A*, 2013, **4**, 999.
7 J. Morales, L. Sánchez, F. Martín, J. R. Ramos-Barrado and M. Sánchez, *Electrochim. Acta*, 2004, **49**, 4589.
8 J. Luo, J. Liu, Z. Zeng, C. F. Ng, L. Ma, H. Zhang, J. Lin, Z. Shen and H. J. Fan, *Nano lett.*, 2013, **13**, 6136.
9 J. Ma, X. Zhang, K. Chen and X. Han, *RSC Adv.*, 2014, **4**, 9166.
10 (a) J. Luo, X. Xia, Y. Luo, C. Guan, J. Liu, X. Qi, C. F. Ng, T. Yu, H. Zhang and H. J. Fan, *Adv. Ener. Mater.*, 2013, **3**, 737; (b) F. Han, D. Li, W.-C. Li, C. Lei, Q. Sun and A.-H. Lu, *Adv. Funct. Mater.*, 2013, **23**, 1692; (c) Z. Wang, L. Zhou and X. W. David Lou, *Adv. Mater.*, 2012, **24**, 1903; (d) B. Koo, H. Xiong, M. D. Slater, V. B. Prakapenka, M. Balasubramanian, P. Podsiadlo, C. S. Johnson, T. Rajh and E. V. Shevchenko, *Nano lett.*, 2012, **12**, 2429; (e) B. P. Hahn, J. W. Long, A. N. Mansour, K. A. Pettigrew, M. S. Osofsky and D. R. Rolison, *Energ. Environ. Sci.*, 2011, **4**, 1495.
11 (a) Z. Wang, D. Luan, S. Madhavi, C. M. Li and X. W. Lou, *Chem Commun.*, 2011, **47**, 8061; (b) Y.-M. Lin, P. R. Abel, A. Heller and C. B. Mullins, *J. Phys. Chem. Lett.*, 2011, **2**, 2885; (c) F. Cheng, J. Liang, Z. Tao and J. Chen, *Adv. Mater.*, 2011, **23**, 1695; (d) J. Zhang, T. Huang, Z. Liu and A. Yu, *Electrochem. Commun.*, 2013, **29**, 17; (e) L. Zhang, H. B. Wu and X. W. D. Lou, *Adv. Ener. Mater.*, 2014, **4**, 1300958.
12 (a) K. Yan, H. W. Lee, T. Gao, G. Zheng, H. Yao, H. Wang, Z. Lu, Y. Zhou, Z. Liang, Z. Liu, S. Chu and Y. Cui, *Nano lett.*, 2014, **14**, 6016; (b) Z. W. Seh, J. H. Yu, W. Li, P. C. Hsu, H. Wang, Y. Sun, H. Yao, Q. Zhang and Y. Cui, *Nat. commun.*, 2014, **5**, 5017; (c) L. Zhou, H. Xu, H. Zhang, J. Yang, S. B. Hartono, K. Qian, J. Zou and C. Yu, *Chem Commun.*, 2013, **49**, 8695; (d) Z. Padashbarmchi, A. H. Hamidian, H. Zhang, L. Zhou, N. Khorasani, M. Kazemzad and C. Yu, *RSC Adv.*, 2015, **5**, 10304.
13 Y. Yin, R. M. Rioux, C. K. Erdonmez, S. Hughes, G. A. Somorjai and A. P. Alivisatos, *Science*, 2004, **304**, 711.
14 H. Zhang, X. Sun, X. Huang and L. Zhou, *Nanoscale*, 2015, **7**, 3270.
15 (a) S. Stankovich, D. A. Dikin, G. H. B. Dommett, K. M. Kohlhaas, E. J. Zimney, E. A. Stach, R. D. Piner, S. T. Nguyen and R. S. Ruoff, *Nature*, 2006, **442**, 282; (b) E. Yoo, J. Kim, E. Hosono, H.-s. Zhou, T. Kudo and I. Honma, *Nano lett.*, 2008, **8**, 2277; (c) C. Wang, D. Li, C. O. Too and G. G. Wallace, *Chem. Mater.*, 2009, **21**, 2604.
16 S. Xiang, W. Zhou, Z. Zhang, M. A. Green, Y. Liu and Chen.B., *Angew. Chem. Int. Edit.*, 2010, **49**, 4615.
17 T. Yamashita and P. Hayes, *Appl. Surf. Sci.*, 2008, **254**, 2441.
18 P. Mills and J. L. Sullivan, *Appl. Phys.*, 1983, **16**, 723.
19 (a) Y. Mizokawa, *J. Vac. Sci. Technol. A*, 1987, **5**, 2809; (b) J. Diaz, G. Paolicelli, S. Ferrer and F. Comin, *Phys. Rev. B*, 1996, **54**, 8064; (c) P. Merel, M. Tabbal, M. Chaker, S. Moisa and J. Margot, *Appl. Surf. Sci.*, 1998, 105; (d) V. Chandra, J. Park, Y. Chun, J. W. Lee, I. C. Hwang and K. S. Kim, *Acs Nano*, 2010, **4**, 3979.
20 M. Hu, A. A. Belik, M. Imura, K. Mibu, Y. Tsujimoto and Y. Yamauchi, *Chem. Mater.*, 2012, **24**, 2698.
21 L. Zhang, H. B. Wu and X. W. Lou, *J. Amer. Chem. Soc.*, 2013, **135**, 10664.
22 (a) Y. Hou, T. Huang, Z. Wen, S. Mao, S. Cui and J. Chen, *Adv. Ener. Mater.*, 2014, **4**, 1400337; (b) Z. He, J. L. Maurice, A. Gohier, C. S. Lee, D. Pribat and C. S. Cojocaru, *Chem. Mater.*, 2011, **23**, 5379.
23 (a) Y. Wu, P. Zhu, M. V. Reddy, B. V. Chowdari and S. Ramakrishna, *ACS Appl. Mater. Inter.*, 2014, **6**, 1951; (b) I. T. Kim, A. Magasinski, K. Jacob, G. Yushin and R. Tannenbaum, *Carbon*, 2013, **52**, 56.
24 (a) Y. Li, C. Zhu, T. Lu, Z. Guo, D. Zhang, J. Ma and S. Zhu, *Carbon*, 2013, **52**, 565; (b) H. Zhang, L. Zhou, O. Noonan, D. J. Martin, A. K. Whittaker and C. Yu, *Adv. Funct. Mater.*, 2014, **24**, 4337; (c) Z. Wang, D. Luan, S. Madhavi, Y. Hu and X. W. Lou, *Energ. Environ. Sci.*, 2012, **5**, 5252; (d) G. W. Zhou, J. Wang, P. Gao, X. Yang, Y. S. He, X. Z. Liao, J. Yang and Z. F. Ma, *Ind. Eng. Chem. Res.*, 2013, **52**, 1197; (e) H. Zhang, L. Zhou and C. Yu, *RSC Adv.*, 2014, **4**, 495.
25 M. M. thackeray, W. I. F. David and J. B. Goodenough, *Mat. Res. Bull.*, 1982, **17**, 785.
26 H. Lindstrom, S. Sodergren, A. Solbrand, H. Sensmo, J. Hjelm, A. Hagfldt and S. E. Lindquist, *J. Phys. Chem. B*, 1997, **101**, 7717.

